The structure of Al_xFeNi phase in Al–Cu–Mg–Fe–Ni alloy (AA2618)

I.N.A. OGUOCHA, S. YANNACOPOULOS*
Department of Mechanical Engineering, University of Saskatchewan, 57 Campus Drive, Saskatoon, Saskatchewan, Canada S7N 5A9

YAN JIN
Room 502, Mechanical Properties Division, Natural Research Institute for Metals, Sengen 1-2-1, Tsukuba, Ibaraki, Japan 305

The structure of the aluminide phase (Al_xFeNi) in cast AA2618 has been investigated by means of electron probe microanalysis and transmission electron microscopy techniques. The Al_xFeNi phase has been determined to have a C-centred monoclinic structure with lattice parameters $a = 0.8673$ nm, $b = 0.9000$ nm, $c = 0.8591$ nm, and $\beta = 83.504°$. It is also shown that the structural formula of the phase varies from particle to particle and is influenced by the aluminium content.

1. Introduction

AA2618 is an Al–Cu–Mg–Fe–Ni forging alloy developed for aircraft engine components and has good elevated temperature strength up to 238 °C [1, 2]. It has been reported that the simultaneous additions of small amounts of iron and nickel result in the formation of insoluble iron- and nickel-rich (aluminide) dispersoid particles [1, 3]. The aluminide phase has been identified as Al_9FeNi phase [1, 3, 4]. Recently, the crystal structure of the Al_9FeNi phase in spray-formed AA2618 has been studied by means of transmission electron microscopy (TEM) and high-resolution electron microscopy (HREM) techniques [3]. It was found to have a primitive monoclinic structure with lattice parameters of $a = 0.6213$ nm, $b = 0.6290$ nm, $c = 0.8557$ nm, and $\beta = 94.76°$. In the present work, it has been observed that the selected-area diffraction patterns (SADPs) of aluminide particles could be indexed consistently using a different model, thus indicating that the particles may possess different crystal structures.

2. Experimental procedure

The material used in this work was cast monolithic AA2618 supplied by Duralcan Inc (San Diego, USA). The chemical composition (wt %) of the alloy is given in Table I. Samples of the as-supplied materials were solution heat-treated at 530 °C for 2 h, water-quenched to room temperature, and aged both naturally and artificially for various lengths of time. Artificial ageing was carried out at 200 °C on samples which had been given prior room-temperature ageing for 40 h. The microstructures of the aged samples were examined by scanning electron microscopy (SEM), electron probe microanalysis (EPMA), and transmission electron microscopy (TEM). The SEM and EPMA samples were metallurgically polished. The SEM samples were examined in a Jeol JXA-840 scanning microanalyser equipped with a SiLi detector and 3 μm thick norvar window. The IPP program, developed by Tracor Northern, was used for image analysis. Further, a Jeol JXA-8600 electron probe microanalyser, equipped with a gas-proportional detector and a windowless detector, was used to analyse different insoluble phases found in the alloy. The Heinrich/Duncumb-Reed correction program was employed.

The samples used for TEM observations were cut from the aged materials by means of a very thin diamond-tipped circular cutter and were subsequently ground using 600-grit emery paper to a thickness of approximately 200 μm. Discs, 3 mm in diameter, were cut from the 200 μm thick materials and a TEM disc grinder was used to reduce further the thickness to about 100 μm. The disc samples were then prepared by both the ion-milling technique and the conventional electro-polishing method. The ion-milled samples were thinned in two stages: (i) the discs were dimpled to a thickness of about 25 μm in a GATAN 656 dimpler grinder using 2–4 μm diamond paste; (ii) the discs were then thinned to perforation using a GATAN 600 dual ion-miller equipped with a cold stage and cooled continuously with liquid nitrogen. An accelerating voltage of 6 V, a total gun current of 1 mA (0.5 mA/gun) and an incident ion-beam angle of 13° were used.

* Author to whom all correspondence should be addressed.

0022–2461

TABLE I Chemical analysis of AA2618

Material	Element									
	Si	Fe	Cu	Mn	Mg	Cr	Ni	Zn	Ti	Al
AA2618	0.18	1.19	2.34	–	1.59	–	1.05	–	0.07	Balance

Electropolishing was done in a solution which contained one part (volume) of 90% commercially pure nitric acid (HNO_3) and three parts of methanol (CH_3OH) and was maintained between -15 and $-50\,^{\circ}C$ at a voltage of 20 V. All thin foils were examined in a Jeol JEM 2000FX transmission electron microscope at an accelerating voltage of 150–160 kV, using a combination of bright-field image (BFI) and dark-field image (DFI) techniques, and selected-area diffraction patterns (SADPs). Chemical composition analysis of phases was determined by the X-ray energy dispersive spectroscopy (EDS) method using the standardless metallurgical thin film (SMTF) program. Tilting of the phases from one orientation to another was carried out in the selected-area diffraction mode by tilting the specimen about two mutually perpendicular axes (X and Y) using a double-tilt holder. The software used in analysing the SADPs was developed by Yan Jin [5].

3. Results and discussion

3.1. Microstructure of iron- and nickel-rich phase

Fig. 1a shows a backscattered electron (BE) image of a typical aged sample of AA2618. The large bright (white) spots indicate insoluble dispersoid phases. Fig. 1b is a TEM dark-field (DF) image of a typical iron- and nickel-rich particle at the matrix grain boundary. Fig. 2a and b show the EDS spectra of a typical iron- and nickel-rich particle and the surrounding matrix, respectively. It is evident from Fig. 2a that the insoluble particles are rich in iron and nickel. Fig. 3a–d are X-ray maps showing iron, nickel, copper and magnesium distributions in overaged AA2618, respectively. The distribution of iron is similar to that of nickel indicating that the dispersoid particles are rich in these two elements. The distributions of magnesium and copper are nearly homogeneous in AA2618, although the areas occupied by the dispersoid particles do not contain magnesium (except on the fringes). The presence of copper in the areas occupied by the particles indicates that they contain a small amount of copper, but not sufficient for one to anticipate a new quaternary Al–Cu–Fe–Ni phase.

The iron- and nickel-rich particles have been reported elsewhere [3, 4] to have a structural formula of Al_9FeNi. Recently, Underhill *et al.* [4] reported the existence of Al_7Cu_4Ni particles in spray-formed AA2618. Zhang and Cantor [3] further identified the Al_9FeNi particles as monoclinic phases with lattice parameters of $a = 0.6213$ nm, $b = 0.629$ nm, $c = 0.8557$ nm, and $\beta = 94.76°$. However, a quantitative EPMA analysis of representative particles (see Table II) did not conform to the Al_9FeNi formula. The fabrication route and post-fabrication processes may be responsible for the differences. Because the structure formulae obtained for the iron- and nickel-rich phase in the present study are different from those reported by Zhang and Cantor [3], it is designated Al_xFeNi phase, for convenience.

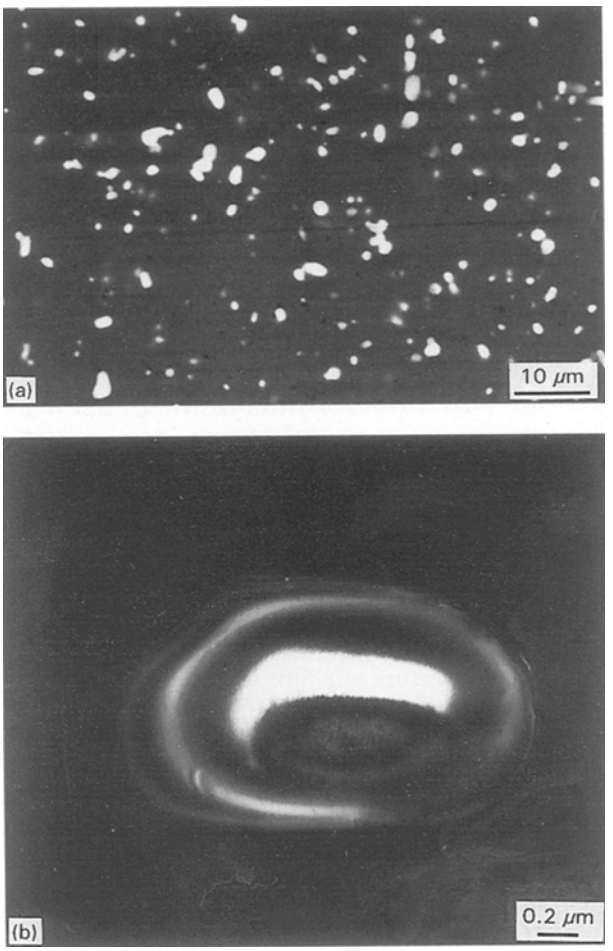

Figure 1 (a) Scanning electron micrograph of solution heat-treated and aged AA2618 showing insoluble dispersoid particles; (b) dark-field TEM image of an iron- and nickel-rich particle at the matrix grain boundary.

As shown in Table II, although x is not the same for all the aluminide particles, the atomic ratio of iron to nickel remains practically consistent at 1:1. Thus, the aluminium content seems to dictate the structure formula of these particles and may alter the crystallography. Further, although the elements found in the iron- and nickel-rich phase were similar to that reported by the previously mentioned investigators [1, 3], some of the SADPs obtained could not be indexed consistently on the basis of the lattice parameters suggested by Zhang and Cantor [3]. That is, the Al_xFeNi phase, is

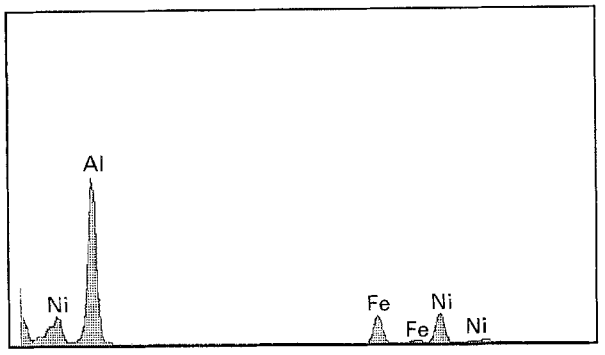

(a)

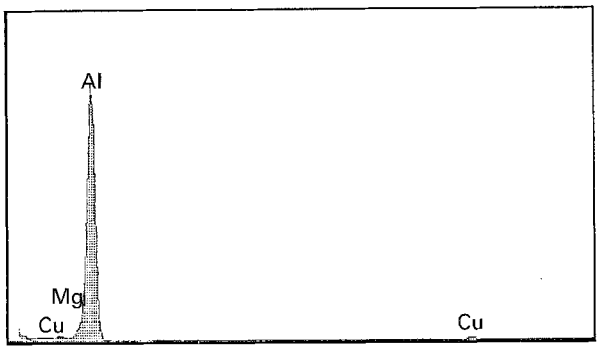

(b)

Figure 2 EDX spectra from (a) Al_xFeNi particle; and (b) the surrounding aluminium matrix.

a primitive monoclinic unit cell with lattice parameters $a = 0.6213$ nm, $b = 0.629$ nm, $c = 0.8557$ nm, and $\beta = 94.76°$. Rather, analysis of SADPs obtained in this study shows that they can be indexed more consistently on the basis of the structure of the Al_x FeNi phase being C-centred monoclinic with $a = 0.8673$ nm; $b = 0.9000$ nm; $c = 0.8591$ nm; and $\beta = 83.504°$. A detailed analysis of the crystal structure of the Al_xFeNi phase, as carried out using the TEM technique, is presented in the following section.

3.2. Crystal structure of Al_xFeNi phase using TEM

It is known that each SADP represents a two-dimensional reciprocal lattice plane. Thus, the three-dimensional reciprocal lattice of a crystal (phase) can be obtained by tilting the crystal systematically along different crystallographic directions. Usually, the operation starts with the specimen oriented in such a way that the zone axis of a high symmetry SADP is parallel to the incident electron beam. The specimen is then tilted along a chosen reciprocal lattice axis in a given direction until the specimen orientation with respect to the electron beam reaches another high-symmetry SADP zone axis. Similar tilting operations are then carried out for other directions. This procedure has been used by many investigators [6–8] for crystal structure determination using the TEM technique. From the results, the three high-symmetry reciprocal lattice planes, which may be perpendicular to each other, will then be selected to form a three-dimensional unit cell of the phase.

Fig. 4a–f are the SADPs of the Al_xFeNi phase obtained by tilting the crystal in one direction, say the MM direction, while Fig. 5a–f are the SADPs obtained by tilting in another direction, say the NN direction. The measured values of these SADPs are shown in Table III, where R_1 and R_2 are the shortest and second shortest vectors of the two-dimensional reciprocal section, respectively, d_1 is the interplanar spacing corresponding to R_1, and θ is the angle between R_1 and R_2. The SADPs in Fig. 4a–f and Fig. 5a–f were indexed using the lattice parameters obtained elsewhere [3] ($a = 0.6213$ nm, $b = 0.629$ nm, $c = 0.8557$ nm, and $\beta = 94.76°$) and the results are shown in Table IV, where $(H_1K_1L_1)$ and $(H_2K_2L_2)$ are the planes corresponding to the two-dimensional reciprocal lattice vectors R_1 and R_2 respectively, while $[U\ V\ W]$ is the direction of the reciprocal lattice plane (that is, the zone axis of the SADP).

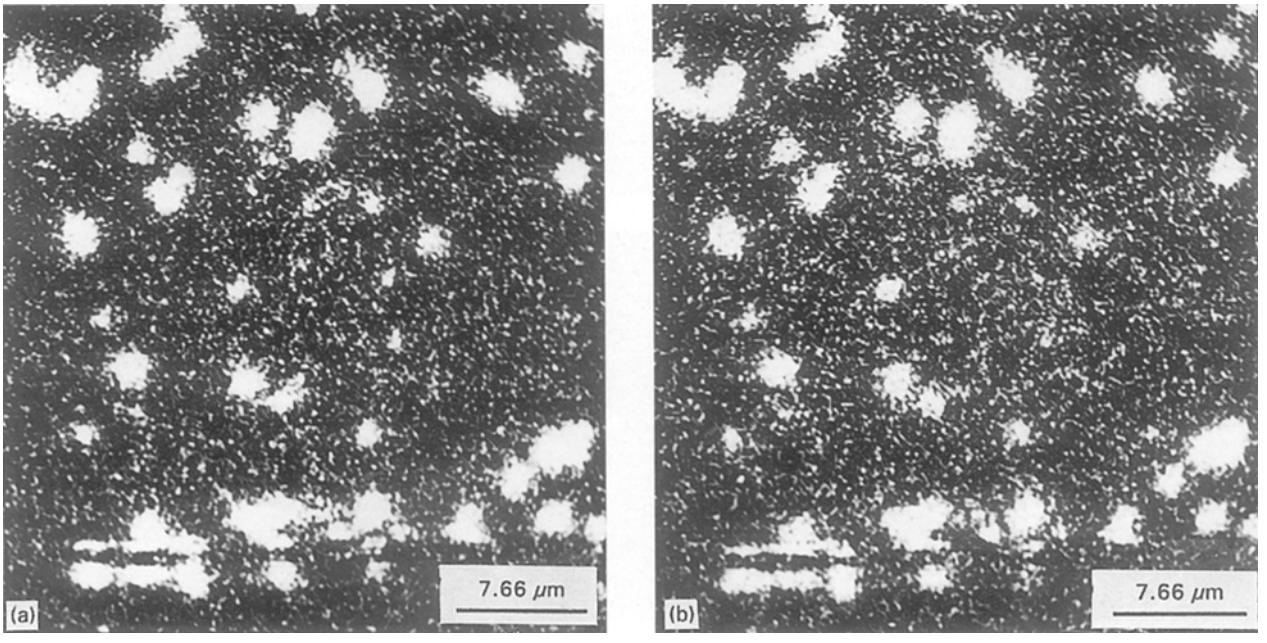

Figure 3 X-ray maps showing (a) iron, (b) nickel, (c) copper, and (d) magnesium distributions in overaged AA2618.

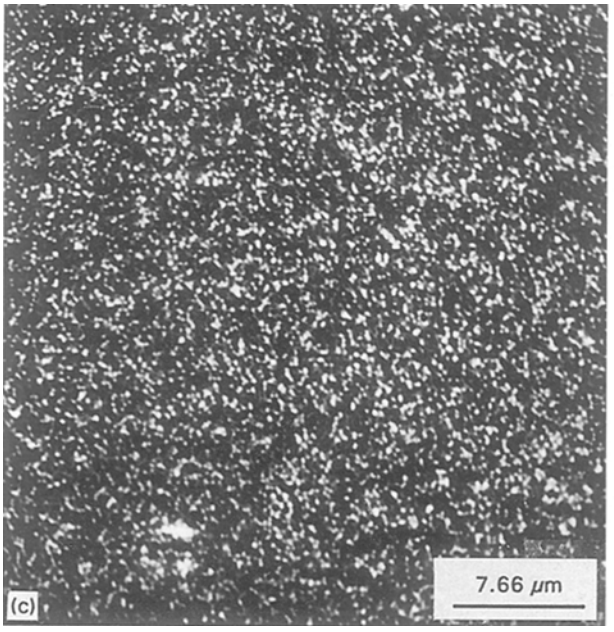

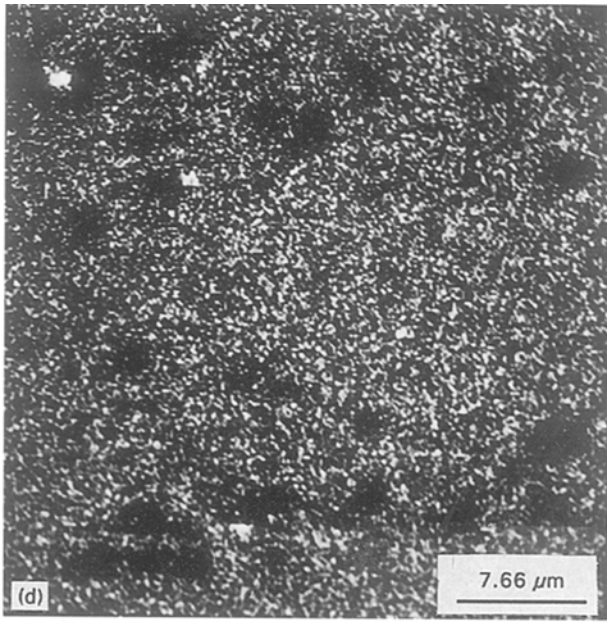

Figure 3 (Continued).

TABLE II EPMA data from Al_xFeNi particles

Particle	Element (wt %)								
	Si	Mn	Fe	Cu	Mg	Ni	Al	Total	Likely phase?
1	0.744	0.02	14.70	1.72	0.153	13.92	68.62	99.88	$Al_{11}FeNi$
2	0.683	0.00	13.75	2.10	0.179	13.80	69.93	100.46	$Al_{11}FeNi$
3	0.460	0.00	9.55	1.91	1.08	9.24	77.75	99.99	$Al_{18}FeNi$
4	0.293	0.03	15.00	1.63	0.418	14.08	68.55	100.00	$Al_{11}FeNi$
5	0.366	0.03	14.83	1.61	0.259	13.78	69.14	100.00	$Al_{11}FeNi$

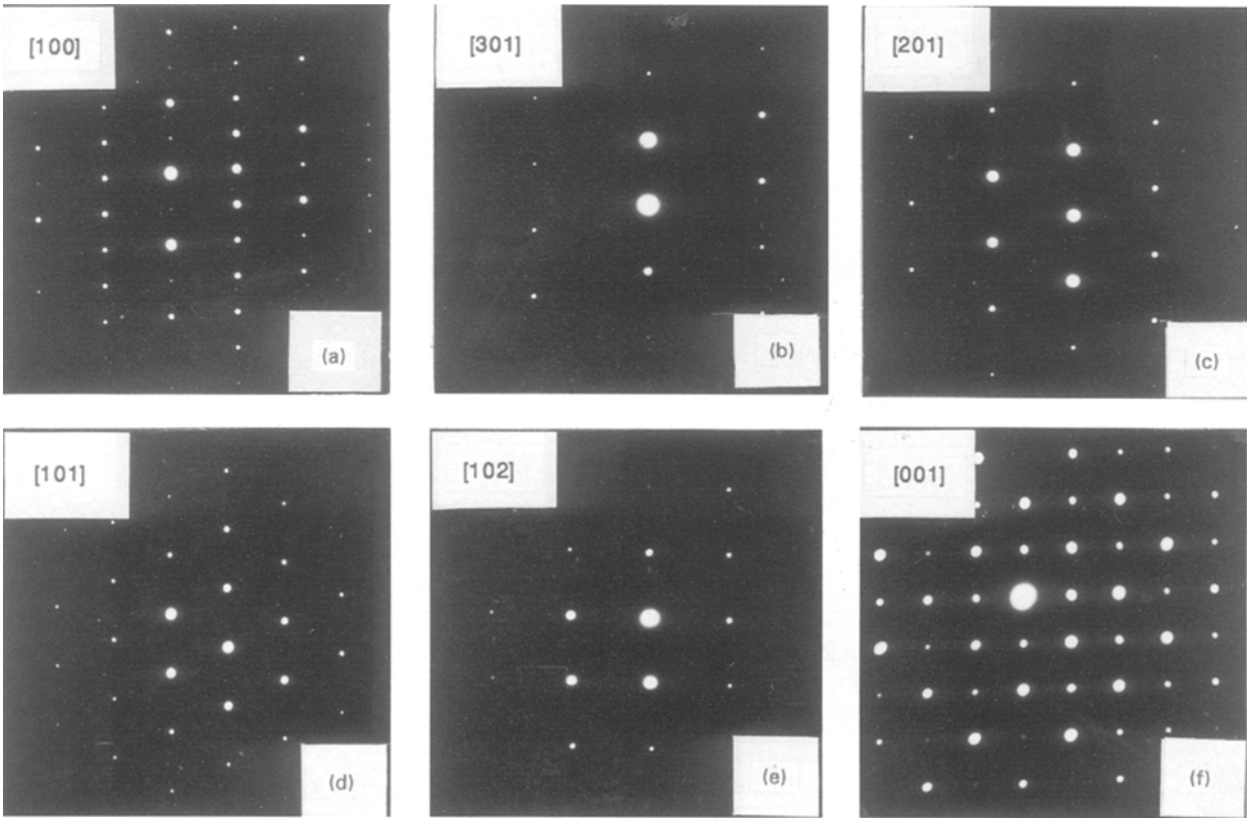

Figure 4 SAD patterns of Al_xFeNi phase obtained by tilting between (a) and (f) ([1 0 0]–[0 0 1] zones).

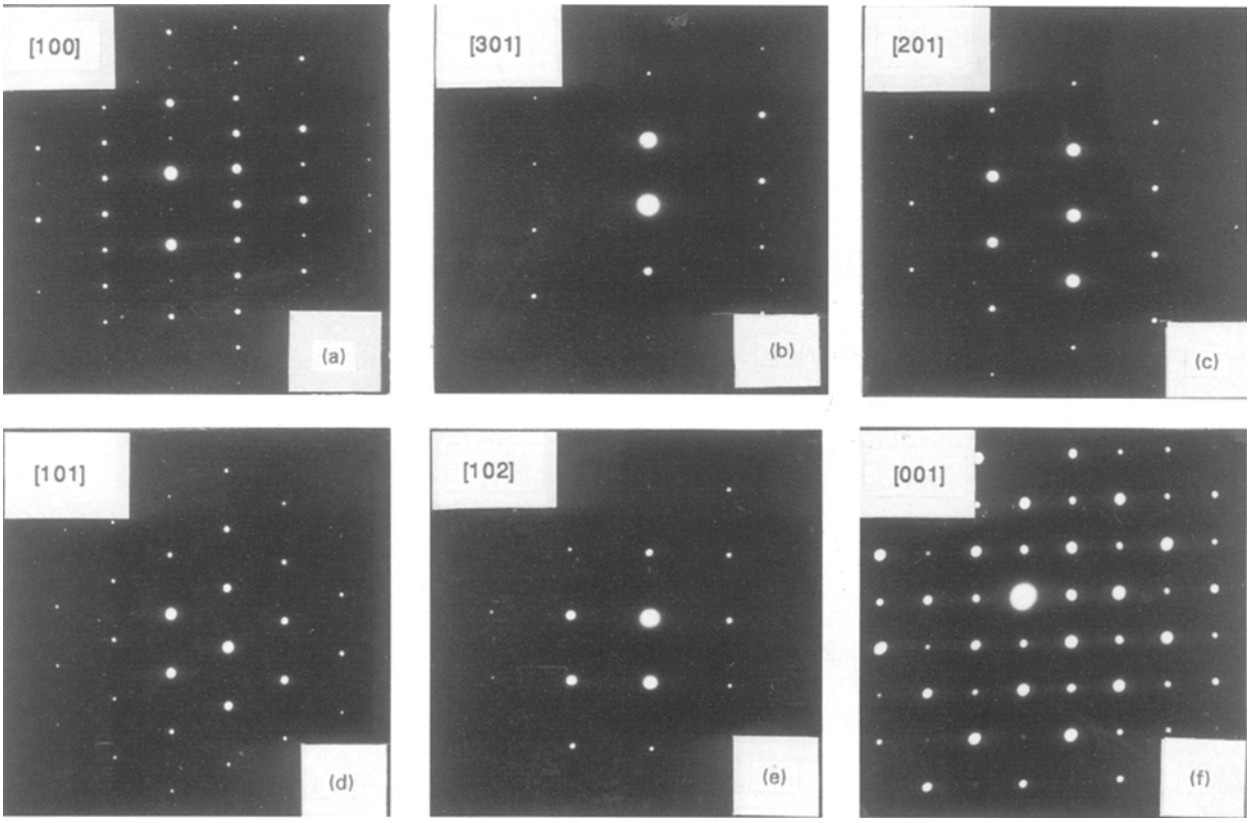

Figure 5 SAD patterns of Al_xFeNi phase obtained by tilting between (a) and (f) ([3 1 0]–[0 1 0] zones).

TABLE III Measured values of the SADPs shown in Figs 4 and 5

	Figure											
	4a	4b	4c	4d	4e	4f	5a	5b	5c	5d	5e	5f
R_2/R_1	1.909	1.794	1.270	1.051	1.210	1.000	3.030	4.2424	1.3636	4.2424	3.030	1.9697
d_1 (nm)	0.8591	0.4500	0.4500	0.4805	0.4500	0.6300	0.8591	0.8591	0.8591	0.8591	0.8591	0.8591
θ (deg)	93 (87)	70	65	55	88	87	91	91.6	93	95	95	96

TABLE IV Calculated and measured values of crystallographic parameters of Al_xFeNi using $a = 0.6213$ nm; $b = 0.6290$ nm; $c = 0.8557$ nm; $\beta = 94.76°$ [3]

Fig.	Measured values			Calculated values			Indices		
	R_2/R_1	d_1 (nm)	θ (deg)	R_2/R_1	d_1 (nm)	θ (deg)	$(H_1K_1L_1)$	$(H_2K_2L_2)$	$[U\,V\,W]$
4a	1.909	0.8591	93	1.932	0.8527	86.6	0 0 1	1 1 0	1–1 0
4b	1.794	0.45	70	1.703	0.4412	76.4	1 1 0	0 1–3	–3 3 1
4c	1.270	0.45	65	1.25	0.4412	69.83	1 1 0	0 1–2	–2 2 1
4d	1.051	0.4805	55	1.049	0.4823	111.97	0 1–1	1 0 1	–1 1 1
4e	1.210	0.45	88	1.152	0.4412	87.69	1 1 0	1–1 1	–1 1 2
4f	1.000	0.6300	87	1.015	0.6289	90	0 1 0	1 0 0	0 0 1
5a	3.030	0.8591	91	3.041	0.8527	87.84	0 0 1	1–2 0	2 1 0
5b	4.242	0.8591	91.6	4.294	0.8527	88.47	0 0 1	1–3 0	3 1 0
5c	1.364	0.8591	93	1.355	0.8527	90.00	0 0 1	0 1 0	1 0 0
5d	4.242	0.8591	95	4.294	0.8527	88.48	0 0 1	1 3 0	3–1 0
5e	3.030	0.8591	95	3.041	0.8527	87.84	0 0 1	1 2 0	2–1 0
5f	1.970	0.8591	96	1.932	0.8527	86.6	0 0 1	1 1 0	1–1 0

The calculated and experimental values of the angle between the zone axes of the SADPs in Figs 4a–f and 5a–f are shown in Table V. One way to verify the consistency and accuracy of the lattice parameters obtained in the previous studies [3] for indexing the Al_xFeNi particle is to compare the experimental and calculated values of the parameters R_2/R_1, d_1, and θ. As shown in Table IV, the measured and calculated angles, in most cases, differ significantly. Further, the calculated inter-angles between the SADPs in Figs

TABLE V Calculated and measured values of angles between the zone axis of the SADPs shown in Figs 4 and 5 ($a = 0.6213$ nm; $b = 0.6290$ nm; $c = 0.8557$ nm; $\beta = 94.76°$ [3])

Serial no.	Orientation	Calculated θ (deg)	Measured θ (deg)
1	−1 1 0 ∧ −3 3 1	17.543	17.104
2	−3 3 1 ∧ −2 2 1	7.623	7.756
3	−2 2 1 ∧ −1 1 1	17.28	16.742
4	−1 1 1 ∧ −1 1 2	17.62	17.725
5	−1 1 2 ∧ 0 0 1	26.594	25.743
6	−1 1 0 ∧ 0 0 1	86.656	83.504
1	2 1 0 ∧ 3 1 0	8.201	8.921
2	3 1 0 ∧ 1 0 0	18.648	18.694
3	1 0 0 ∧ 3 −1 0	18.648	18.235
4	3 −1 0 ∧ 2 −1 0	8.201	8.530
5	2 −1 0 ∧ 1 −1 0	18.505	18.597
6	2 1 0 ∧ 1 −1 0	72.2	68.016

TABLE VII Calculated and measured values of angles between the zone axis of the SADPs shown in Figs 3 and 4 based on C-centred monoclinic structure ($a = 0.8673$ nm; $b = 0.9000$ nm; $c = 0.8591$ nm; $\beta = 83.504°$)

Serial no.	Orientation	Calculated θ (deg)	Measured θ (deg)
1	1 0 0 ∧ 3 0 1	17.549	17.104
2	3 0 1 ∧ 2 0 1	7.435	7.756
3	2 0 1 ∧ 1 0 1	16.524	16.742
4	1 0 1 ∧ 1 0 2	16.613	17.725
5	1 0 2 ∧ 0 0 1	25.381	25.743
6	1 0 0 ∧ 0 0 1	83.504	83.504
1	3 1 0 ∧ 2 1 0	8.342	8.921
2	2 1 0 ∧ 1 1 0	18.637	18.694
3	1 1 0 ∧ 1 2 0	18.213	18.235
4	1 2 0 ∧ 1 3 0	7.918	8.530
5	1 3 0 ∧ 0 1 0	17.808	18.597
6	3 1 0 ∧ 0 1 0	70.919	68.016

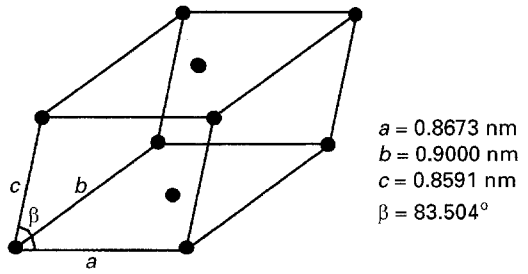

Figure 6 Crystal structure of the Al_xFeNi phase based on the C-centred model.

4a–f and 5a–f with the corresponding experimental values are compared. From the upper section of Table V, it can be seen that the experimental and calculated values of the angles between the zone axes of the SADPs in Fig. 4 are in fairly good agreement with each other but the calculated angle between Fig. 4a and f, that is, between [−1 1 0] and [1 0 0], is not in good agreement with the measured value. From the lower section of Table V, a similar observation can be made for Fig. 5a and f.

Because the SADPs in Figs 4 and 5 could not be completely indexed with the lattice parameters suggested by Zhang and Cantor [3], it became necessary to establish a more consistent model for the Al_xFeNi phase. Using the measured values in Table IV and a computer-based SADP analysis program [5], it was determined that the Al_xFeNi phase has a monoclinic structure with lattice parameters $a = 0.8673$ nm, $b = 0.900$ nm, $c = 0.8591$ nm, and $\beta = 83.504°$. The three reciprocal lattice planes shown in Figs 4a, f, and 5f were chosen to form a three-dimensional unit cell of the Al_xFeNi phase. The three-dimensional reconstruction of these SADPs (i.e. those corresponding to the [1 0 0], [0 0 1], and [0 1 0] zone axes) suggests that the Al_xFeNi phase is a C-centred monoclinic. The real lattice crystal structure of the Al_xFeNi phase which corresponds to the latter structure is also carbon-centred monoclinic with lattice parameters as mentioned above. This is shown in Fig. 6. The indexed patterns corresponding to the [1 0 0], [0 0 1], and [0 1 0] zone axes are shown schematically in Fig. 7a–c. Table VI shows the results of the calculations. As usual, $(H_1K_1L_1)$ and $(H_2K_2L_2)$ are the planes corresponding to R_1 and R_2 which are the shortest and second shortest vectors of the two-dimensional reciprocal lattice plane, respectively, and θ is the angle between R_1 and R_2. $[U\ V\ W]$ is the zone axis of the SADP. It can

TABLE VI Calculated and measured values of crystallographic parameters of Al_xFeNi phase based on C-centred structure ($a = 0.8673$ nm; $b = 0.9000$ nm; $c = 0.8591$ nm; $\beta = 83.504°$)

Fig.	Measured			Calculated			Indices		
	R_2/R_1	d_1 (nm)	θ (deg)	R_2/R_1	d_1 (nm)	θ (deg)	$(H_1K_1L_1)$	$(H_2K_2L_2)$	$[U\ VW]$
4a	1.909	0.8591	93	1.896	0.8535	90.00	0 0 1	0 2 0	1 0 0
4b	1.794	0.45	70	1.791	0.4499	73.79	0 2 0	1 1–3	3 0 1
4c	1.270	0.45	65	1.326	0.4499	67.85	0 2 0	1 1–2	2 0 1
4d	1.051	0.4805	55	1.000	0.4844	65.12	1 1–1	1–1–1	1 0 1
4e	1.210	0.45	88	1.222	0.4499	90.00	0 2 0	2 0–1	1 0 2
4f	1.000	0.6300	87	1.000	0.6224	87.51	1 1 0	1–1 0	0 0 1
5a	3.030	0.8591	91	3.012	0.8535	92.13	0 0 1	1–3 0	3 1 0
5b	4.242	0.8591	91.6	4.279	0.8535	93.00	0 0 1	2–4 0	2 1 0
5c	1.364	0.8591	93	1.371	0.8535	94.68	0 0 1	1–1 0	1 1 0
5d	4.242	0.8591	95	4.392	0.8535	95.85	0 0 1	4–2 0	1 2 0
5e	3.030	0.8591	95	3.119	0.8535	96.18	0 0 1	3–1 0	1 3 0
5f	1.970	0.8591	96	1.981	0.8535	96.49	0 0 1	2 0 0	0 1 0

TABLE VIII Reflection conditions of Al_xFeNi phase and possible point and space groups

Reflection conditions	$(h\,0\,0)$	$(0\,k\,0)$	$(0\,0\,l)$	$(h\,k\,0)$	$(0\,k\,l)$	$(h\,0\,l)$	$(h\,k\,l)$
	$h = 2n$	$k = 2n$	None	$h + k = 2n$	$k = 2n$	$h = 2n$	None
Point group	2	m	$2/m$				
Space groups	C2	Cm	C2/m				

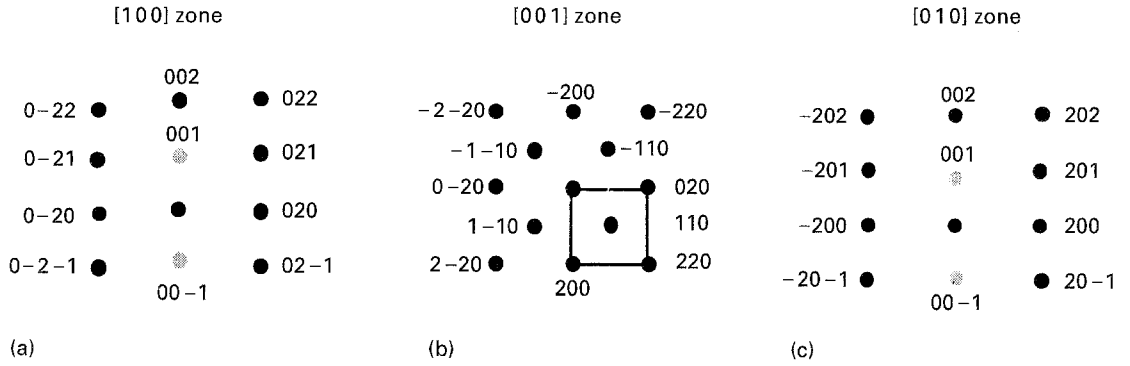

Figure 7 Indexed patterns of Figs 4a, f, and 5f.

be seen that the calculated values are fairly consistent with the experimental values. Again, if the above lattice parameters are correct, the calculated angles between the zone axis of the SADPs in Figs 4 and 5, should be consistent with the corresponding experimental values. Table VII shows the comparison. It can be seen from Tables VI and VII that the results are generally satisfactory. Further, the standard seven reflection conditions of the SADPs shown in Figs 4 and 5 were determined. These are given in Table VIII. It is important to note that double reflection conditions seem to have occurred in some SADPs at the (0 0 1) positions (see Figs 4a and 5f and Fig. 7a and 7c). Barring possible errors in the observation of double reflection, the possible point groups and space groups of the Al_xFeNi phase were then determined from the relationship between the seven reflection conditions and the crystal symmetry as obtained form the International Tables for Crystallography [9]. The results are also shown in Table VIII.

4. Conclusions

The results of the present work show that the structural formulae of the iron- and nickel-rich particles in AA2618 are not the same for all particles. They seem to depend on the aluminium content. Finally, the Al_xFeNi phase has been determined to have a carbon-centred monoclinic structure with lattice parameters $a = 0.8673$ nm, $b = 0.9000$ nm, $c = 0.8591$ nm, and $\beta = 83.504°$.

Acknowledgements

The authors thank Duralcan Aluminium Company, San Diego (USA), for the test materials, Mr Tom Klimowicz for assistance and technical discussion, Mr Tom Bonli, Geology Department, University of Saskatchewan, Saskatoon (Canada), for assistance with the EPMA, and Dr M.C. Chaturvedi and his research group, University of Manitoba, Winnipeg (Canada), for assistance with TEM and X-ray mapping equipment. Financial assistance from the Natural Sciences and Engineering Research Council of Canada (NSERC) in the form of a research grant to S. Yannacopoulos is hereby acknowledged.

References

1. R. N. WILSON and P. J. E. FORSYTH, *J. Inst. Metals* **94** (1966) 8.
2. W. A. ANDERSON, "Precipitation Hardening Aluminium Alloys", Precipitation From Solid Solution (ASM, OH, 1957).
3. D. L. ZHANG and B. CANTOR, in "Proceedings of the 2nd European Conference on Advanced Materials and Processes", edited by T. W. Cline and P. J. Withers (University of Cambridge, 1991) p. 197.
4. R. P. UNDERHILL, P. S. GRANT and B. CANTOR, *Mater. Design* **14**(1) (1993) 45.
5. YAN JIN, "TEM Assistant" (version 3.0), Institute of Aeronautical Materials, Beijing 100095, People's Republic of China, 1992.
6. K. YANG, MIN-HSIUNG HONAND KUO-CHANG SU, *Scripta Metall. Mater.* **24** (1990) 953.
7. YAN JIN, CHUNZHI LI, JIAWEI MI and MINGGAO YAN, *Mater. Lett.* **14** (1992) 285.
8. JIN YAN, LI CHUNZHI, MI JIAWEI and YAN MINGGAO, *J. Mater. Sci.* **28** (1993) 6000.
9. T. HAHN, "International Tables for Crystallography', Vol. A, Space Group Symmetry", (Reidel, Dorrecht, Holland, Boston, USA, 1983).

Received 20 September 1995
and accepted 15 January 1996